

Extension related to a high topography: results from a microearthquake survey in the Andes of Peru and tectonic implications

Jacques Deverchère*, Catherine Dorbath† and Louis Dorbath†

* Laboratoire de Géophysique, Bâtiment 509, UA du CNRS 730, Université Paris-Sud, 91405 Orsay Cedex, France and † ORSTOM, 213 rue Lafayette, 75480 Paris Cedex 10, and Institut de Physique du Globe de Strasbourg, 5 rue René Descartes, 67084 Strasbourg, France

Accepted 1989 February 6. Received 1989 February 2; in original form 1988 April 11

SUMMARY

A microearthquake study performed in 1985 October–November in the Cordillera Blanca (western Cordillera of northern Peru) allowed us to make a precise mapping of its shallow seismicity. 160 local events are accurately located in the vicinity of an active normal fault system showing a vertical displacement of 4500 m over the last 7 Myr. Part of the seismic activity can be related to this west-dipping system, but a great number of events indicate a new seismic zone situated under the highest peaks of the chain. By using an inversion algorithm of *P*-wave polarities, we show a regional deviatoric stress tensor which defines an extensional axis in a direction approximately orthogonal to the Andean structures. This result is in good agreement with the theoretical distribution of stresses expected in an elongated high topography bordered by tectonic convergent zones. Moreover, we suggest that an absolute uplift of this young batholith occurs on a normal fault system and that this phenomenon is partly due to buoyancy forces originating in its crustal root.

Key words: intraplate seismicity, active fault, extension, Andes, Peru, stress tensor, gravitational body force

1 INTRODUCTION

Evidence of an extensional state of stress has been reported in many parts of the highest chains in the world. The case of the Tibetan plateau is particularly well documented: both seismological data and microtectonic measurements indicate present extension in a direction roughly perpendicular to the direction of convergence of the Indian and Asian plates (Molnar & Tapponnier 1978; Armijo, Carey & Cisternas 1986; Mercier *et al.* 1987). North and south of the Tibetan plateau, active thrust-faulting occurs at low altitudes. Such an extensional tectonic regime is well explained by extrusion movements in response to the northward push of India in a subduction–collision cycle (Tapponnier, Peltzer & Armijo 1986).

In contrast, the Andean mountain belt is not as well understood. Its tectonic setting displays some similarities with the Himalayan one: the range is bordered on both sides by areas of lower elevation showing a compressional tectonic regime: to the west we have the contact between the Nazca and the South American plates (Chinn & Isacks 1983; Jordan *et al.* 1983), and to the east the boundary between the foot of the Andes and the Amazonian shield (Suarez, Molnar & Burchfiel 1983; Dorbath *et al.* 1986). However, a main difference between the two mountain belts is that no major continental collision has occurred during the history of the Andes (Dalziel 1986; Mégard 1987).

In this context, knowledge of the present state of stress in the high Andes is of great importance to understand why and how crustal thickening occurs. A great limitation for such a study is the scarcity of major crustal events in the Cordillera (Stauder 1975; Suarez *et al.* 1983). Moreover, field studies report different tectonic styles: while thrust faulting seems to be prevalent in the eastern Cordillera, normal faulting has been documented in a number of localities in the high Andes, generally on faults trending in a direction parallel to the belt (Suarez *et al.* 1983; Sébrier *et al.* 1985). Strike–slip movements can also be important in the chain and may well have been underestimated by authors. The most spectacular example of an extensional regime is the Cordillera Blanca, in the northern part of the Peruvian western Cordillera (Dalmayrac 1974; Yonekura *et al.* 1979; Dalmayrac & Molnar 1981).

The purpose of this paper is to describe the results obtained in the Cordillera Blanca from a microearthquake study and to deduce some information on the state of stress in this high range of the central Andes.

2 GEOLOGICAL SETTING OF THE CORDILLERA BLANCA

The Cordillera Blanca is 200 km long, it has a general N145°E direction and lies in the western Cordillera of northern Peru, between latitudes 8.5°S and 10.3°S (Fig. 1).

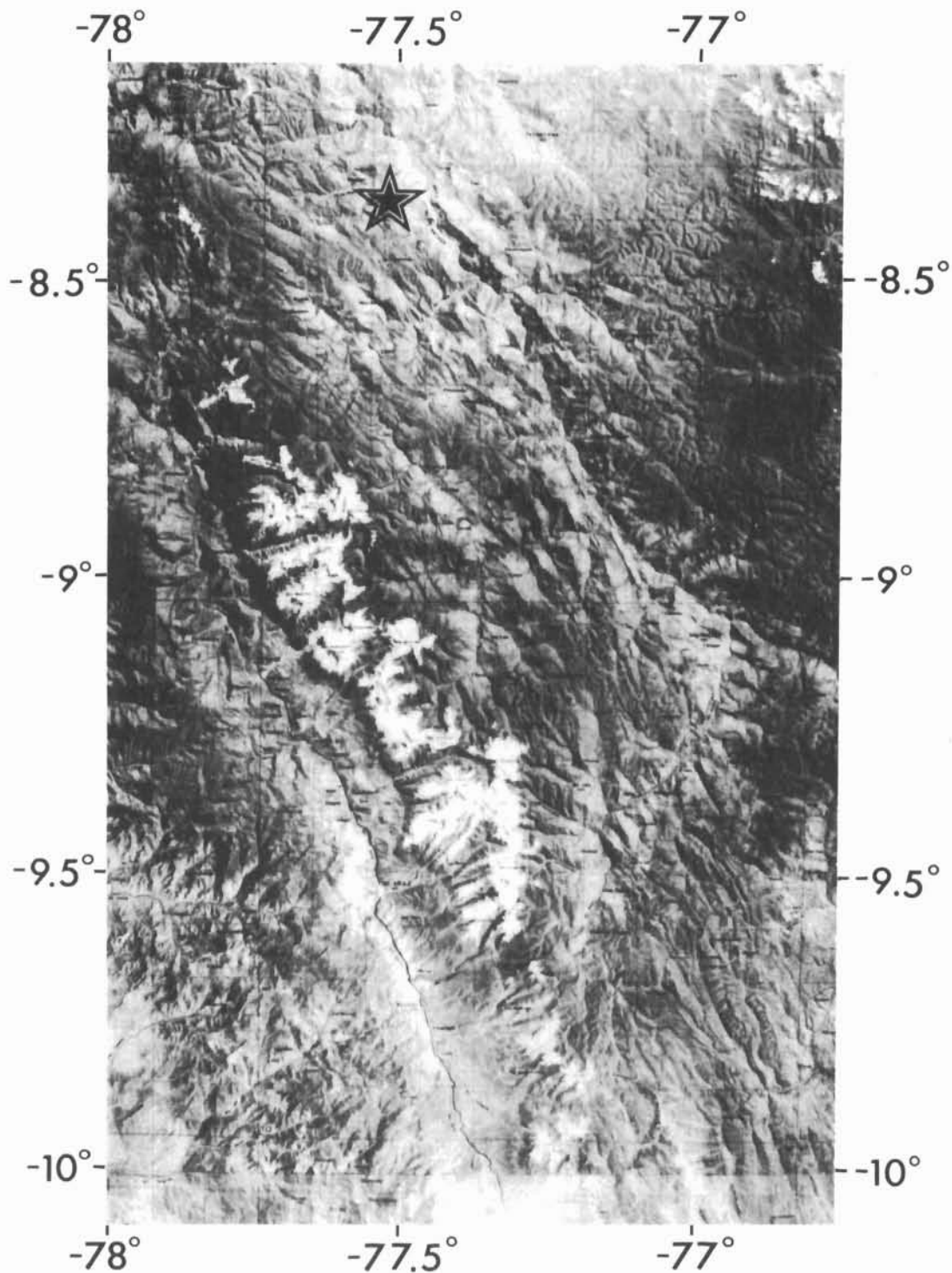


Figure 1. Landsat composite image of the western Cordillera of Peru between 8 and 10°S. Snow-capped range is the Cordillera Blanca batholith. Steep escarpment to the west of the range displays zone of normal fault. Star indicates the epicentral region of the 1946 November 10, Ancash earthquake.

Such a snow-capped range, with altitudes reaching 6800 m (Nevado Huascarán), is quite uncommon and suggests that its relief is very young. We observe a vertical variation of 4 km across the range over a distance of 15 km, thus showing one of the steepest gradients in the Andes.

The Cordillera Blanca consists of a very narrow and linear granodioritic batholith (Fig. 2). Age determinations on its

intrusive rocks give values ranging from 9 to 12 Myr (Giletti & Day 1968; Stewart, Evernden & Snelling 1974). It is much younger than the Coastal Batholith, a main intrusive feature of the late Cretaceous and Paleogene age (Cobbing & Pitcher 1972) extending more to the west between the coast and the western Cordillera (Fig. 2). To the east, the Cordillera Blanca batholith gently disappears under the

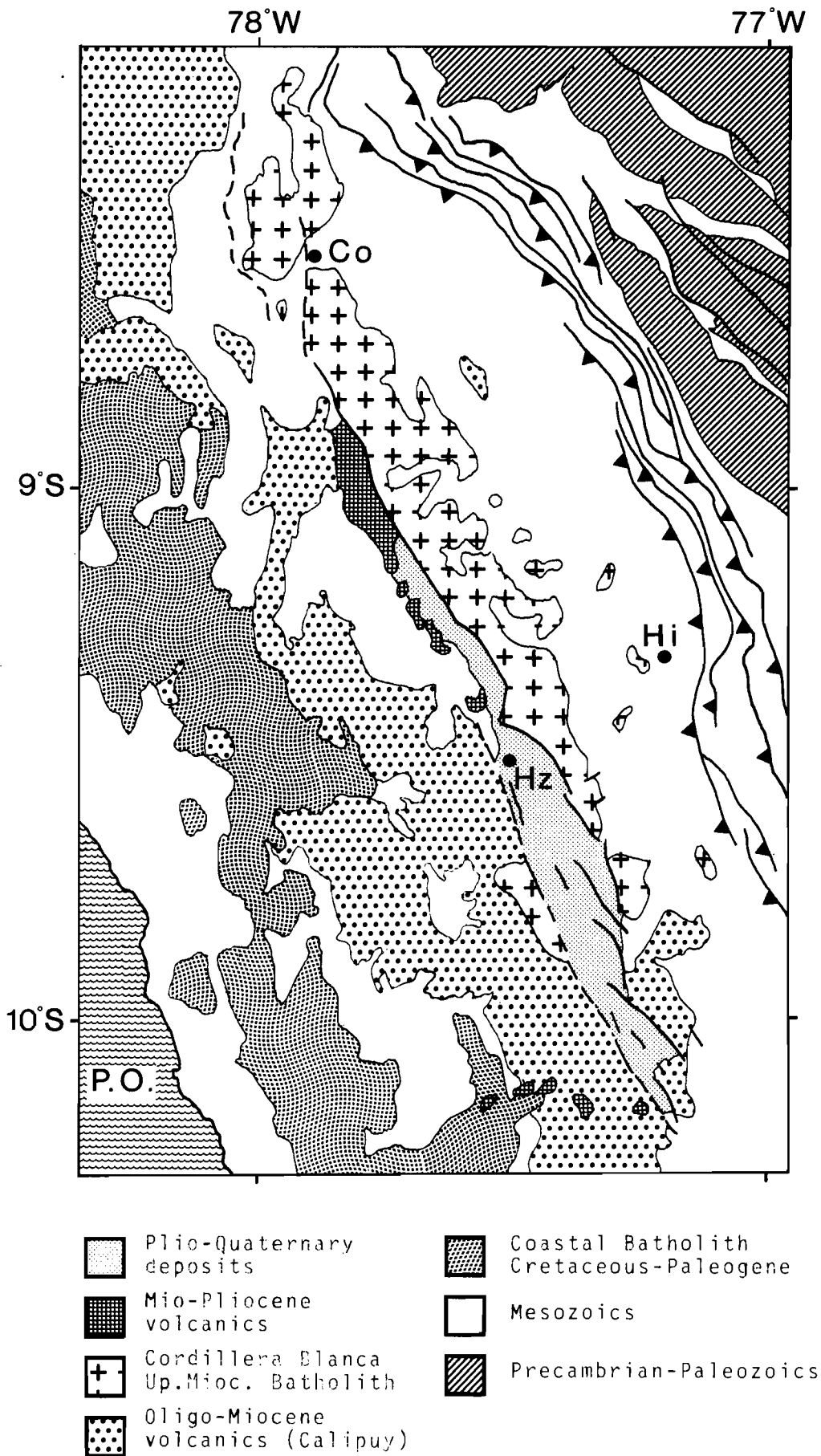


Figure 2. Geologic map of the Cordillera Blanca zone (after Bonnot 1984). Location in Peru is shown on Fig. 4. Hz: Huaraz; Hi: Huari; Co: Corongo; P.O.: Pacific Ocean.

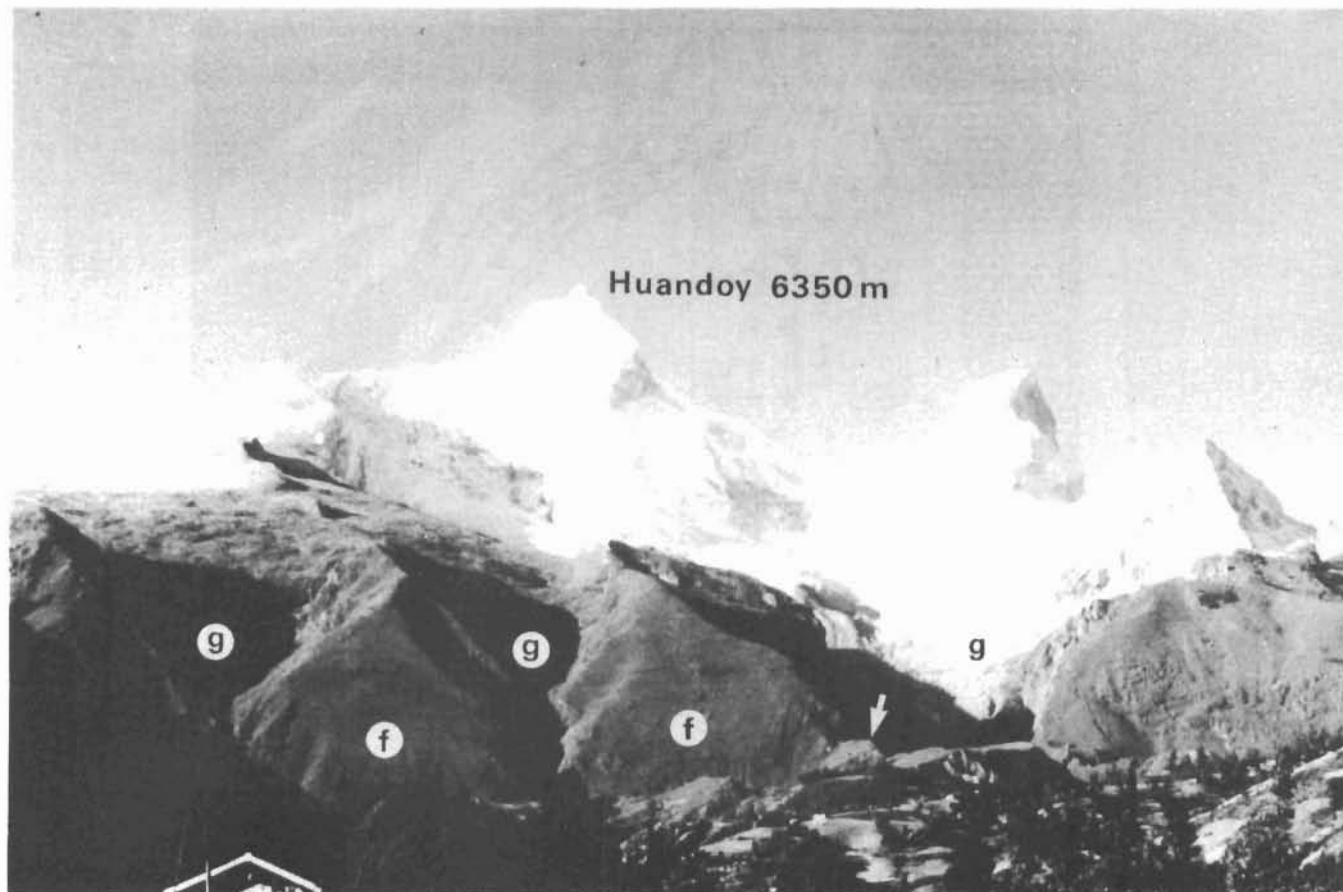


Figure 3. Photograph of the Nevado Huandoy fault scarps taken 5 km north of Yungay (see Fig. 4), in the Rio Santa basin, at an elevation of 2800 m. Fault plane is cut by glacial valleys (g) and forms triangular facets (f) 1000 m high. Late Quaternary moraines are offset about 60 m at the foot of the scarp (white arrow).

Mesozoic sedimentary cover which has been intensely folded and thrust during the main Andean orogenesis of middle and late Eocene age. This structural unit is called the Marañon Fold and Thrust Belt (Wilson, Reyes & Garayar 1967; Mégard 1984). To the west, a very abrupt normal fault zone separates the batholith from a Plio–Quaternary depression, the Callejon de Huaylas basin (Figs 1 and 2).

This fault system is remarkable by its magnitude and length and it has been studied by several authors (Dalmayrac 1978; Yonekura *et al.* 1979; Bonnot 1984). In its northern part, it looks as a very simple fault which trends N145°E, is 80 km long and has a visible throw of about 1000 m (Fig. 3). Its direction changes abruptly from N145°E to N195°E over 10 km to the north of Huaraz. An 8 km long segment striking N110°E again cuts the fault trace direction, marking off a geometrical asperity (Fig. 1). To the south, the fault again strikes about N145°E, but in the form of a left-hand 'en échelon' system. The individual 'en échelon' scarps have a maximum length of 15 km and extend partly into the basin. The total Plio–Quaternary throw is distributed among them.

The Callejon de Huaylas basin is about 12 km wide and is mainly filled with Pliocene deposits. Altitude varies from 4.5 km at the south to 2.5 km at the north. It reaches a maximum width of 18 km and a maximum thickness of 2 km in its southern part (Bonnot 1984). The depression is limited

to the west by the Cordillera Negra chain which has a mean altitude of 4500 m and is mainly formed by thick volcanics of Oligo–Miocene age called the Calipuy formation (Wilson *et al.* 1967). The boundary between the Cordillera Negra and the basin is marked south of Huaraz by a linear fault (Fig. 2) which seems to have been inactive for the past 2 Myr (Bonnot 1984).

With regard to the Pliocene period (7–2 Myr), there is general agreement to recognize an extensional regime in a direction roughly orthogonal to the Cordillera Blanca. This is shown by a relative vertical displacement of about 3500 m on the fault system. Simultaneously, the basin seems to have worked as a graben where several hundred meters of sediments were deposited (Bonnot 1984). Quaternary sedimentation is very weak or absent, but relative uplift of the batholith still went on, giving rise to triangular scarps 1000 m high (Fig. 3). At the foot of these scarps, morphological scarplets offset late Quaternary moraines at some places (Yonekura *et al.* 1979; Bonnot 1984). For the Quaternary period, two interpretations founded on slickensides observations, are proposed: Dalmayrac & Molnar (1981) depict an extension approximately in the same direction N65°E (i.e. orthogonal to the range) during the whole uplift history of the Cordillera Blanca, while Bonnot (1984) distinguishes two main directions of extension: a first one normal to the range during Pliocene time and a second

one nearly N-S since 2 Myr. A seismological study might resolve these conflicting points of view.

3 DATA AND PROCEDURES FOR LOCATING EARTHQUAKES

The data used here are *P*- and *S*-wave arrival times from earthquakes recorded by a temporary regional network. We had both to cover an extended region and to precisely detect superficial activity: for these reasons we installed 11 portable instruments at a mean distance of 20 km within and around the Cordillera Blanca (Fig. 4) in order to obtain a precise image of the seismic activity at shallow depths. The stations used were Sprengnether MEQ 800 portable instruments connected to vertical L4C seismometers. They worked continuously during 34 days in 1985 October–November. Procedures used during the field work were similar to those described, e.g. by Grange *et al.* (1984) in southern Peru. Some of the characteristics of our network were the following:

- (i) All our stations used smoke paper recordings.
- (ii) A careful choice of sites allowed us to set the gain of most instruments at 84 dB.
- (iii) Time marks were made every second.
- (iv) The drifts of all clocks, accurately checked using a WWV broadcast system, were linear and smaller than 0.03 s day^{-1} .

Due to these good recording conditions and the proximity of events (very clear impulsive arrivals), we estimate that uncertainties in arrival times for most earthquakes are generally less than 0.05 s (0.05 mm on the seismograms) for *P*-waves and 0.5 s for *S*-waves. To locate the hypocentres, we used the HYPOINVERSE routine (Klein 1978) modified to allow for differences in station elevations in calculating travel times. First we chose a velocity model based on previous works (James 1971; Couch *et al.* 1978; Cunningham, Roecker & Hatzfeld 1986). Then, in order to take into account the local geology, we modified the superficial velocity structures at each station, especially at those situated in the graben. We finally kept the reasonable velocity structure that gave smallest rms residuals and errors in depth and epicentre (see Table 1). The value of V_P/V_S ratio (1.70 ± 0.01) was deduced from the plot of *P* travel time versus *S*–*P* travel time (Wadati plot), and the trial depth was 10 km. According to the network configuration (Fig. 4), we defined the following criteria for selecting the most reliable locations (class A):

- (i) Each earthquake had eight or more phases including at least one *S*-wave arrival time: in fact, all selected events have at least two *S*-wave readings.
- (ii) The rms value of travel time residuals was less than 0.40 s.
- (iii) The calculated horizontal error (erh) and vertical error (erz) were less than 5 km.
- (iv) The condition number of the matrix of hypocentre partial derivatives (i.e. the ratio of highest eigenvalue to lowest eigenvalue) was less than 100 (see Cunningham *et al.* 1986).

We added a few less reliable locations (class B) which slightly differ from these criteria by a erz value greater than 5 km but generally smaller than 20 km and by a number of

phases equal to six or seven with at least one *S*-wave phase, and showing a good stability.

We obtained 160 well determined crustal earthquakes within the network or very close to it: 124 belonged to class A, 36 to class B. In fact, 76 per cent of events have a rms < 0.2 s, 84 per cent a horizontal error erh < 2 km and 80 per cent a vertical error erz < 4 km. In order to estimate the real uncertainties on depths and epicentres, we made tests on a few characteristic events by introducing reasonable changes on the following parameters: *P*-wave surface velocities, depths of layers, model distribution, V_P/V_S ratio and trial depth. As usual, depth is the most sensitive parameter; but we never observed changes greater than 4 km for class A and 8 km for class B events.

In order to check the effect of systematic station residuals on the hypocentres, we plotted station delays for three different groups of earthquakes: the group around station VES (79 events), the group around station TIN (16 events) and the group around station ISI (14 events) (Fig. 4). Then we recomputed the events using these mean station residuals as station delays: the dispersion of epicentres is slightly reduced and the central cluster of the band (2) is more pronounced.

Finally, we estimate that the precision of most of the 160 locations is better than 4 km in depth and 2 km in epicentral coordinates. These estimates are reasonable if we compare them with those of Grange *et al.* (1984) who found 7 and 3 km, respectively, for shallow events, but with a less dense network. Such a detailed study on hypocentre reliability was necessary to obtain the precise relation of events with the main fault surface.

4 SEISMICITY

The seismic activity is mainly concentrated in the northern half of the array (Fig. 4). It appears as three narrow seismic bands about 30 km long and a few kilometers wide, with a direction roughly parallel to the local structures. The first band (1) extends west of the main fault, between the stations MIT and ISI and seems to change direction to the south (Fig. 4). The two other seismic lines are located east of the main fault; the central one (2) is the most active. Distances separating the first band, the fault and bands (2) and (3) are 10, 5 and 6 km (Fig. 4). These values are quite significant because they are greater than the maximum estimated uncertainty of epicentres. It is worthy to note that the three seismic bands, especially the first one, end where the main change in the fault direction occurs (see above). This pattern of seismicity leads us to remark that this geometrical change might constitute a barrier (Aki 1984).

On a central cross-section orthogonal to the structures (Fig. 5), we observe that nearly all hypocentres are between 0 and 10 km. This result suggests that the brittle part of the crust is rather thin, like in other high plateaus and mountain belts in the world (Chen & Molnar 1983). In contrast, 200 km south-east of this area, in the subandean zone, crustal events reach 30 km (Dorbath *et al.* 1986).

Figure 5 also suggests that under the basin, at least the first 2 km are aseismic: this zone corresponds to the Pliocene sediments. The arrow on the cross-section indicates the foot of the scarp at the surface. As the fault dips 45° to the west,

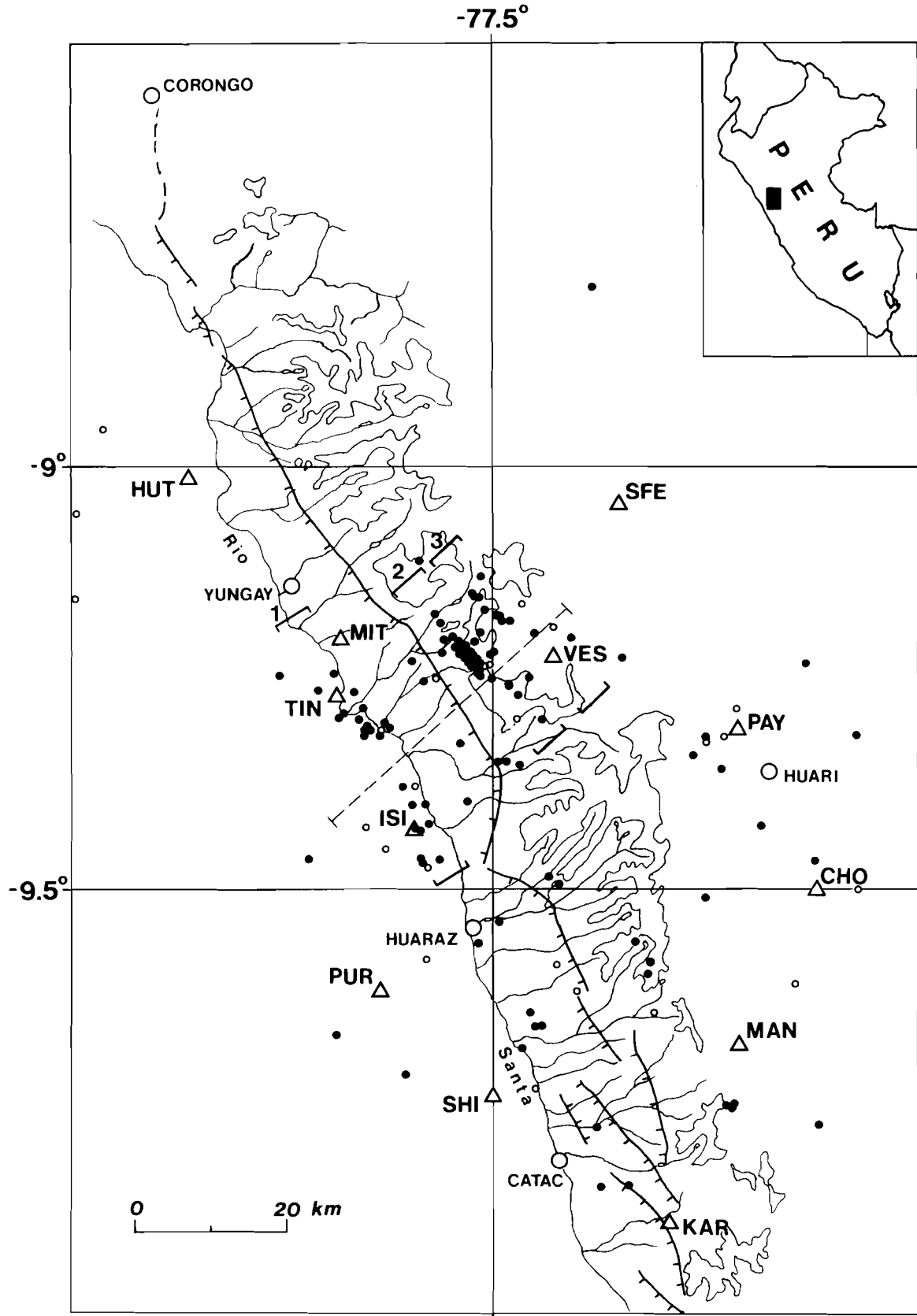


Figure 4. Seismicity map of the local events of the Cordillera Blanca recorded during 34 days. A hundred and fifty shocks are plotted. Triangles are stations. TIN has been moved to MIT after 15 days. The main fault system is represented by barbed lines. Magnitudes of events are between 0.5 and 3.2. Solid squares: A events. Open squares: B events (only 25 are inside this map). The central seismic bands (1, 2 and 3) include 109 events and are plotted after relocation (see text). Contour lines mark the altitude of 5000 m. The river system of Rio Santa is delineated. Dashed line indicates the location of the cross section of Fig. 5.

Table 1. Velocity models.

HUT, MIT, TIN, ISI	Other stations
0 km	0 km
4.8 km s ⁻¹	5.7 km s ⁻¹
2 km	8 km
5.7 km s ⁻¹	6.3 km s ⁻¹
10 km	25 km
6.3 km s ⁻¹	6.7 km s ⁻¹
25 km	50 km
6.7 km s ⁻¹	8.0 km s ⁻¹
50 km	
8.0 km s ⁻¹	

a great deal of events of the western band (1) are slightly above the prolongation of the fault into the crust: they depict a general west dipping pattern. Surprisingly, the most active group is the central one (2), at about 10 km east of the fault trace, just below the highest peaks (Fig. 4). It displays a very dense cluster located at 5 ± 2 km depth. Since the uncertainty in depth is 4 km, it is difficult to define a precise geometry for this group, but it appears approximately vertical.

In the southern part of the Cordillera Blanca, seismicity is much less abundant and more diffuse, although it is well covered by the network (Fig. 4). No obvious pattern appears, except that seismicity remains in the vicinity of the fault system. North of the array, from Yungay to at least 9°S, seismicity is very weak or absent (except west of station HUT, in the Cordillera Negra): this part of the main fault system was quite quiescent during our study.

5 STRESS TENSOR AND FAULT PLANE SOLUTIONS

Recently, various numerical methods have been proposed to determine a regional stress tensor using focal mechanisms of earthquakes (e.g. Gephart & Forsyth 1984; Carey-Gailhardis & Mercier 1987). Here, we used a numerical method developed by Rivera & Cisternas (1987) based on inversion of *P*-wave polarities of a population of earthquakes to estimate both the orientation and shape of the stress tensor, and the individual fault plane solutions. The output of the inverse problem produces a stress tensor (or more than one) explaining the observed set of polarities for all earthquakes and all stations. Thus we obtain by this method the stress tensor not from already determined focal mechanisms, but from the original data of polarities and take-off angles used to calculate them. The individual focal mechanisms come out as a by-product of the calculations: fault plane parameters are chosen to maximize the agreement between observed and theoretical signs of first motions, and this is done by using the probability model of Brillinger, Udias & Bolt (1980). However, in the method we use, the focal mechanisms are individual and are related only by the compatibility with the stress tensor first determined.

We selected all events within the network or very close to it with six *P*-wave polarities or more. Of the sample, 49 earthquakes responded to this criteria; only two were

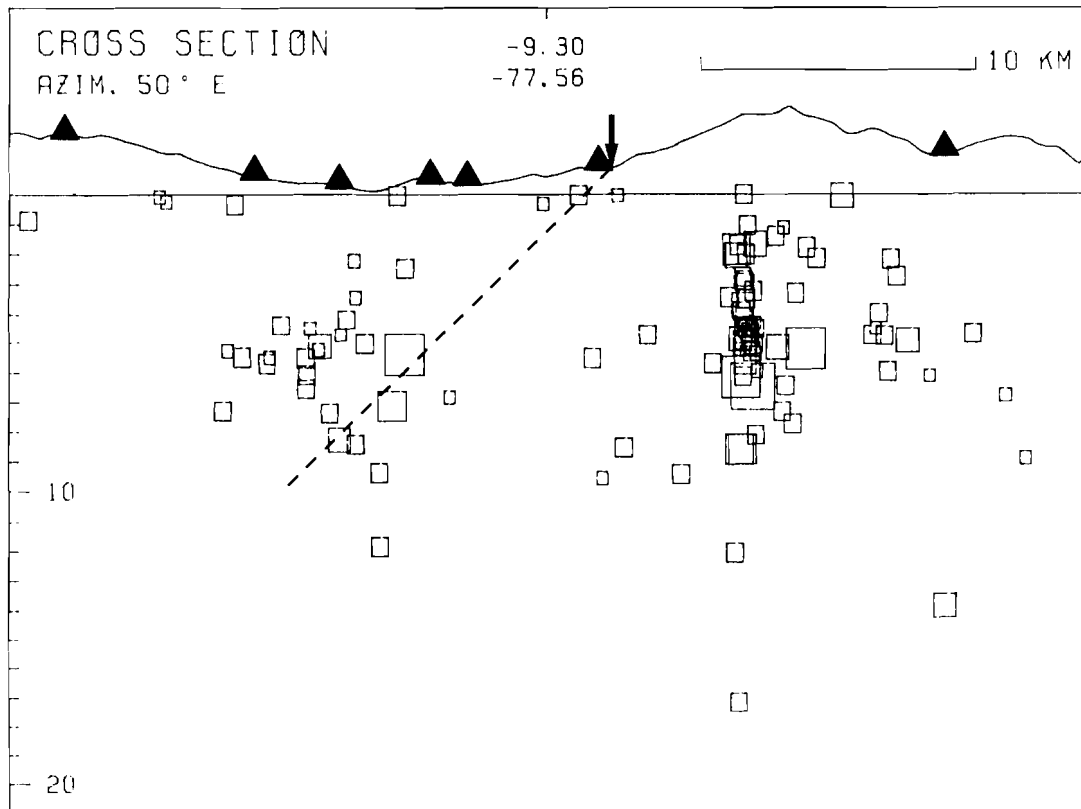


Figure 5. Cross-section perpendicular to the three seismic bands (see Fig. 4). 109 events are projected. Squares are proportional to the magnitudes of events. Black arrow indicates the fault trace at the surface and dashed line the prolongation of the fault dip into the crust. The horizontal line is the reference level of the velocity model, i.e. 2600 m, altitude of the lowest station. Triangles are stations.

eliminated because they were clearly not compatible with the others. As the method is strongly non-linear, it is necessary to provide a trial tensor close to the 'true' one in order to converge quickly and to obtain the optimal solution. With this purpose, we first built individual focal mechanisms with the best documented events by using both graphical and numerical methods (Brillinger *et al.* 1980) and we obtained the best trial tensor by the method of the P and T dihedra (Angelier & Mechler 1977): this tensor is extensional with an horizontal minimal principal stress striking N45°E. Then we carefully explored the possibilities around this trial tensor. We also tested the one proposed by Bonnot (1984) with a minimal principal stress striking N-S as a trial tensor, but it gave a very poor solution. Two calculated tensors correctly explain our data (Fig. 6):

(i) The first one (T1) is extensional: the shape factor R

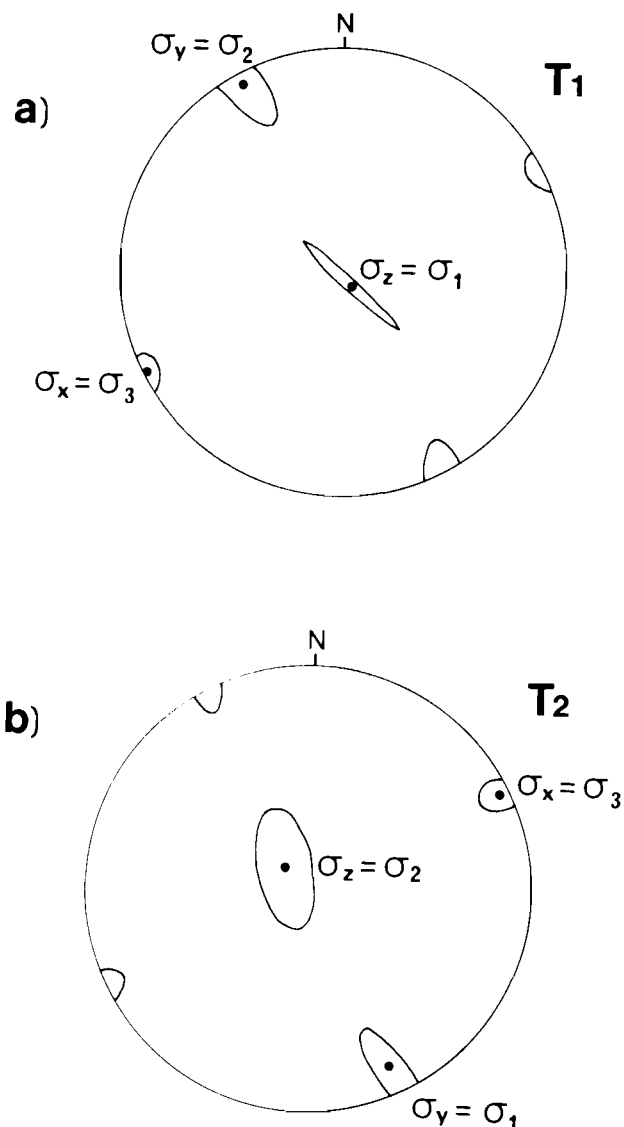


Figure 6. Orientation of the principal axes of the two stress tensors determined by the numerical method. σ_x , σ_y and σ_z are the eigenvalues of the stress tensors. σ_1 , σ_2 and σ_3 refer to the maximum, intermediate and minimum principal stress, respectively. The ellipses correspond to the standard deviation of the axes. Lower hemisphere Schmidt projection is used. a: extensional stress tensor T1; b: strike-slip stress tensor T2.

(Armijo *et al.* 1982) is greater than 1, so $\sigma_z > \sigma_y > \sigma_x$ ($R = \sigma_z - \sigma_x / \sigma_y - \sigma_x$, with $\sigma_y > \sigma_x$). The minimal principal stress σ_x strikes N60°E and the maximal principal stress σ_z is vertical (Fig. 6a). This tensor explains 91 per cent of the observed polarities, i.e. 346/380.

(ii) The second one (T2) corresponds to a strike-slip type: R is between 0 and 1, so $\sigma_y > \sigma_z > \sigma_x$. The maximal principal stress, which was vertical in T1, is now horizontal (Fig. 6b). This tensor explains 90 per cent of the data, i.e. 342/380.

Note that in both cases the minimal principal stress σ_x has the same orientation N60°E (Fig. 6).

Figure 7 indicates the fault plane solution and the slip vector determined by the computation of the tensor T1 for the 47 selected earthquakes. They are located on Fig. 8. The two tensors give nearly the same fault plane solution for each event, except for four of them (7, 12, 14, 27), and these solutions are comparable to those determined before by the graphical and numerical methods. How can an extensional tensor (T1) and a strike-slip tensor (T2) lead to nearly the same mechanisms? It can be easily explained if we observe that most focal mechanisms have a nodal plane close to the azimuth of the principal stress axis σ_y , i.e. N150°E (see Figs 6 and 7). Furthermore, the R value of T1 (1.1 ± 0.3) is very close to 1, which is the boundary value between a strike-slip tensor and an extensional one: in the case of T1, σ_y is the neutral axis, and in the case of T2, it becomes the maximal stress axis (Fig. 6). This means that σ_y and σ_z have very close values. Consequently, as T1 is a solution, the tensor obtained by rotation of 90° around σ_x will also be a solution. This property is apparent in the shape of the error ellipses of axes (Fig. 6): these ellipses are clearly elongated in the direction $\sigma_y - \sigma_z$.

We have observed that σ_y lies in the general direction of the structures (N150°E) and that the minimal principal stress σ_x is orthogonal to this direction (Fig. 6). Such a pattern cannot be attributed to a geometrical artifact, since the fault plane azimuths range widely over more than 100° (Fig. 7): therefore the directions of σ_x and σ_y we found are not the T and B axes, as it should be the case for a monodirectional sample of planes, but are the principal directions of the stress tensor (McKenzie 1969).

No major event has taken place in the area of the study during the last decades. However, a large one occurred on 1946 November 10, known as the Ancash earthquake, 60 km north of the Cordillera Blanca (Fig. 1). This event produced major surface ruptures which have been studied by Silgado (1951). Recently, Suarez *et al.* (1983), by using first motion polarities, and Doser (1987), by modelling long period P -waves of various seismograms, have established a focal mechanism of this earthquake (Fig. 9). The two solutions are very similar and purely extensional: this result confirms the observations of Silgado who described a purely vertical displacement on a 3.5 m scarp high dipping S-W. If we apply the tensor T1 to the fault described by Silgado, we obtain a focal mechanism quite comparable to the one deduced from inversion of Rayleigh waves (Jimenez, Cara & Rouland 1989, see Fig. 9). Both show a very dominant normal component, which corroborates the field observations of Silgado. Thus, our computed results are quite compatible with the prior results on the Ancash earthquake.

In the presence of high relief, many authors justify a

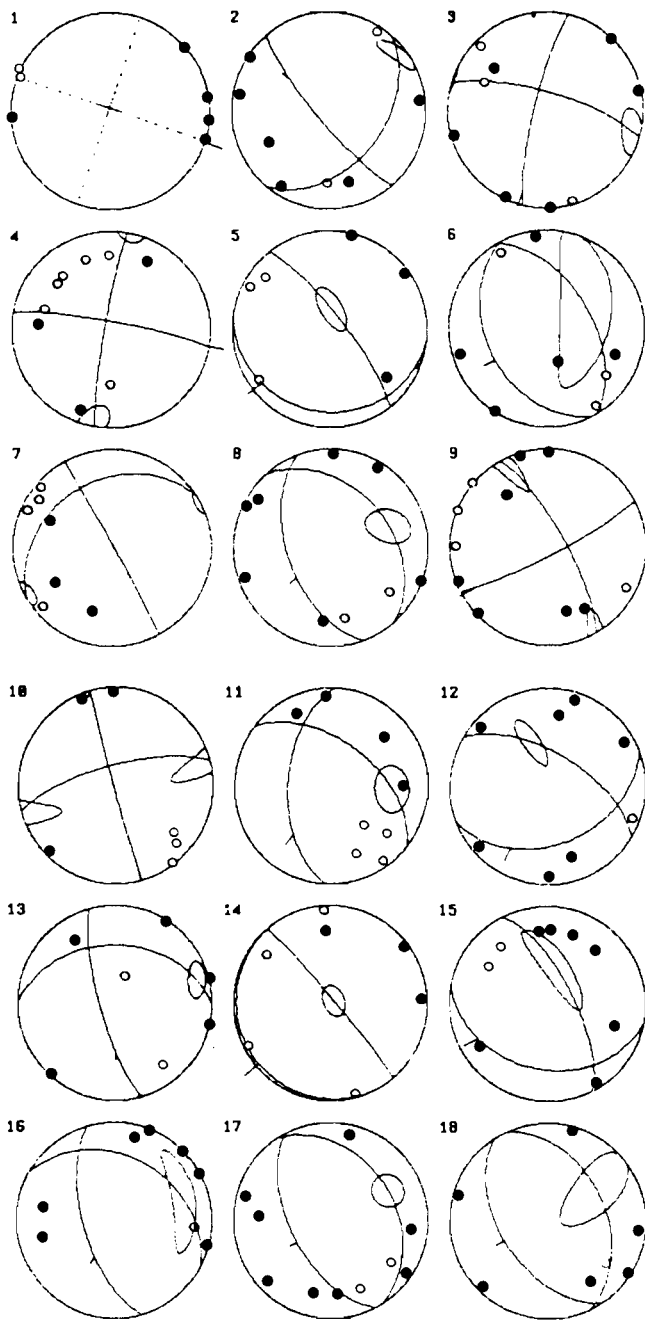
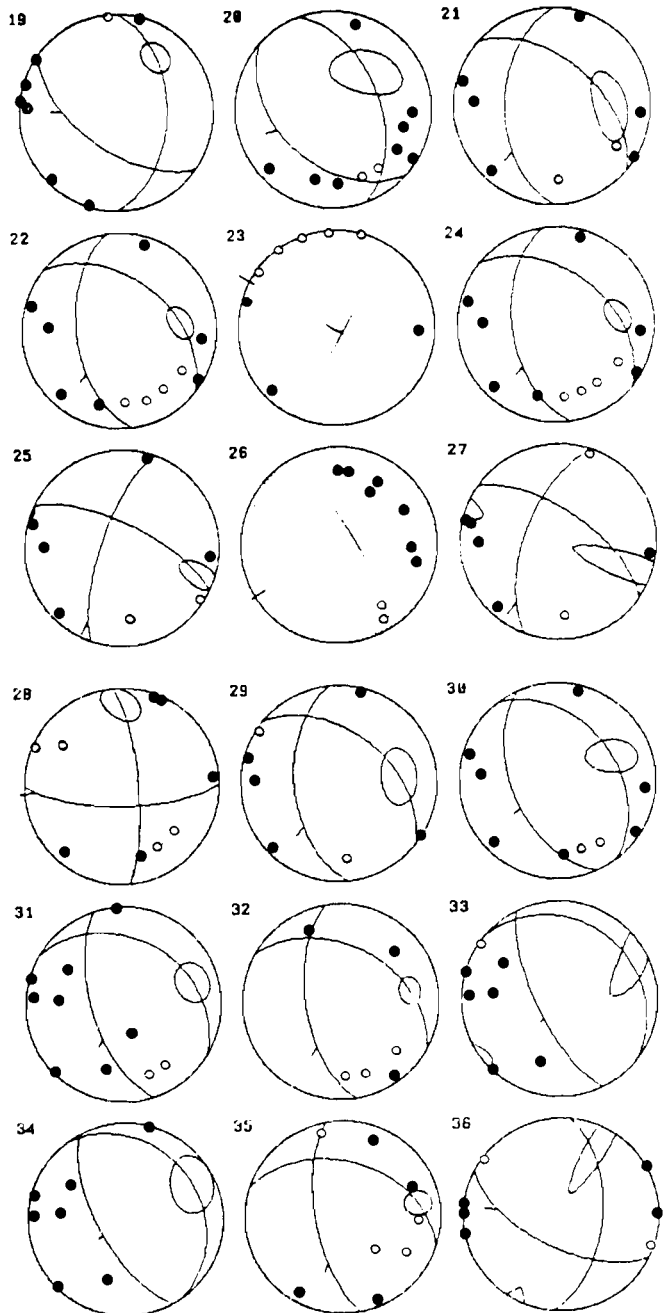


Figure 7. Individual focal mechanisms and fault plane solutions compatible with the extensional stress tensor T1 for the 47 selected events. These mechanisms come out as a by-product of the determination of the stress tensor (see text). Small bars indicate slip vectors on the fault planes. Ellipses show the standard deviation for the poles of the fault planes. Nodal planes are dotted when they are poorly constrained. Lower hemisphere Schmidt projection is used. White: dilatational; black: compressional first motions.

maximal vertical stress by variations in the stress field due to the gravitational body force acting on the high mountains and their crustal roots: this is the case, for example, in the Andes (Dalmayrac & Molnar 1981; Suarez *et al.* 1983; Froidevaux & Isacks 1984; Sébrier *et al.* 1985). Therefore, our result of extensional tensor T1 (which best explains our data) is consistent with this model.

6 DISCUSSION

The most significant result of this microseismic study is the evidence of an active extension in the Cordillera Blanca range in a direction roughly perpendicular to the chain. This is in good agreement with some field observations: Dalmayrac & Molnar (1981) inferred an extensional regime normal to the belt, which is well explained by our tensor T1. Mégard & Philip (1976) and then Soulas (1978), from more detailed studies, deduced an extension in a direction N55°E and a compression in the strike of the Cordillera, which is well explained by our tensor T2. Therefore, from these field works, the same ambiguity between a strike-slip tensor and an extensional tensor appears, as we described before. The



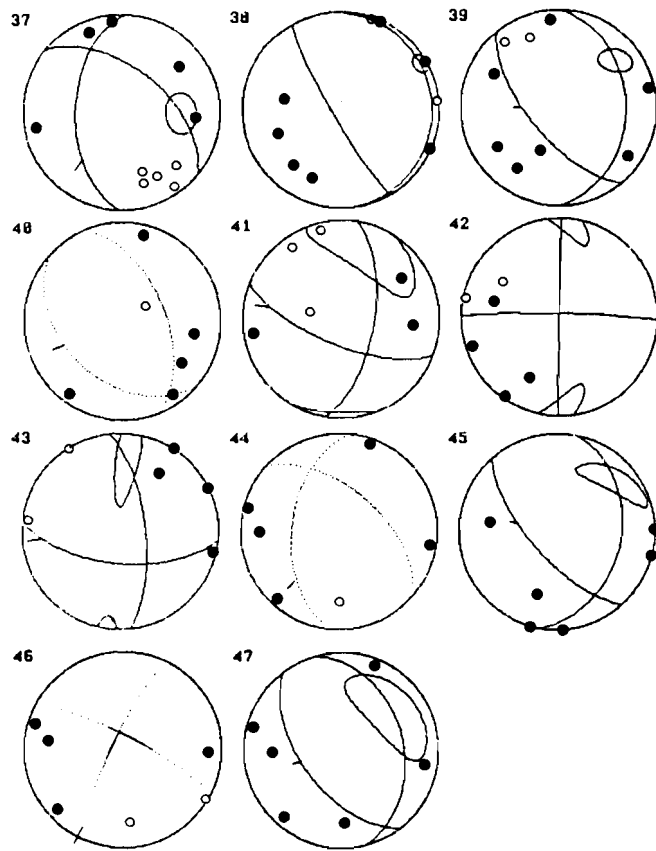


Figure 7 (continued)

-77.50

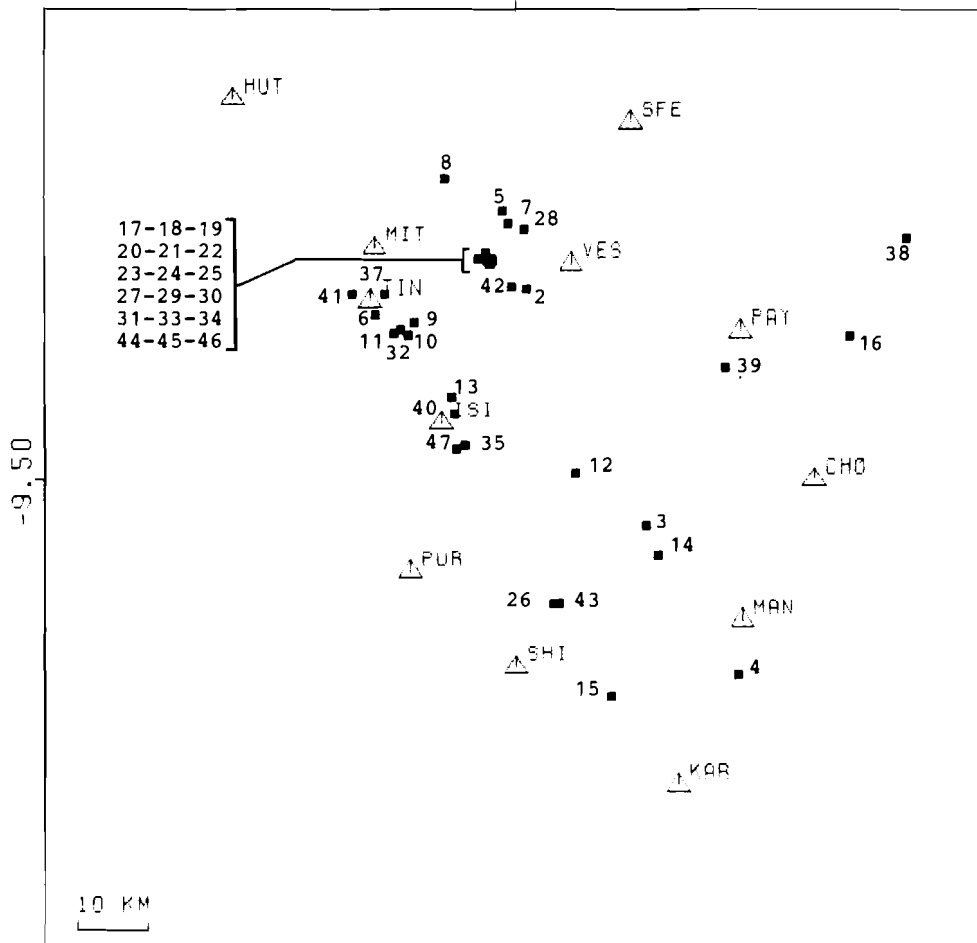


Figure 8. Location of 45 selected events used to determine the stress tensor. Numbers refer to the focal mechanisms represented in Fig. 7. Events 1 and 36 are not represented because they are further to the west.

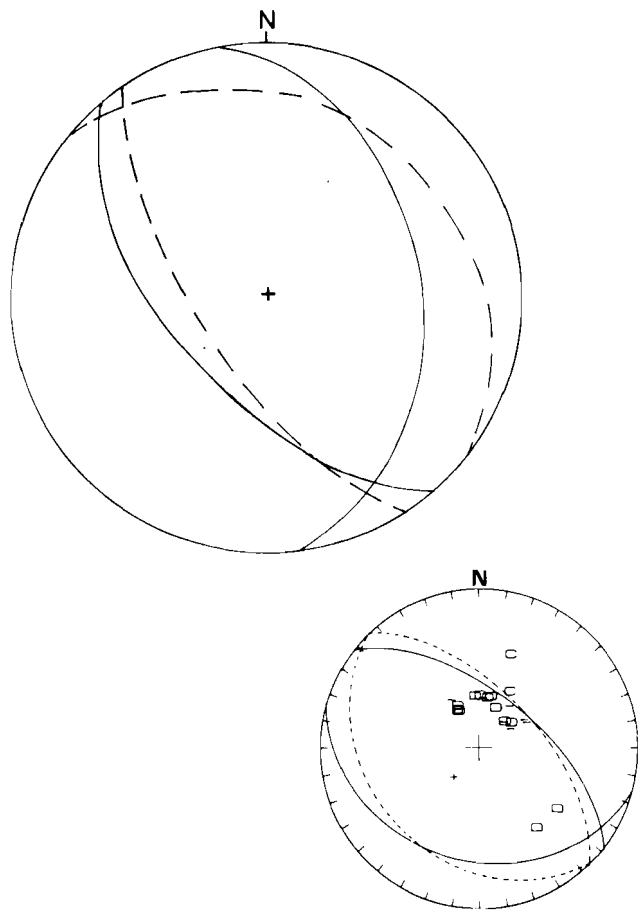


Figure 9. Comparison of focal mechanisms of the 1946 November 10, Ancash earthquake computed using two different techniques (see text). The solid line is the solution obtained by applying tensor T1 to the fault plane described by Silgado (1951). The dashed line is the mechanism obtained by inversion of Rayleigh waves using Paris-St-Maur seismograms (Jimenez, Cara & Rouland 1989). We have added the solutions determined by Doser (1987) at the bottom of the figure: the solid line is the one obtained by waveform modelling; the dashed line is the mechanism from first-motion data. Impulsive compressions and dilatations are denoted by C and D, emergent compressions and dilatations by + and -.

best constrained results owing to Bonnot (1984) for the Quaternary period differ from this frame: according to these slickenside observations, the extensional axis trends 40° more to the north than the one we determined. We have no obvious solution to explain such a discrepancy: we may invoke the effect of a R ratio close to 1 (uniaxial extension), which could disperse slickenside directions, or heterogeneities in stress drop along a major fault zone. Nevertheless, Bonnot's analysis indicates that most of the recent surrection of the Cordillera Blanca (3500/4500 m) occurred in a NE-SW extensional tectonic regime, i.e. the one we inferred from our seismological study. Moreover, our result is consistent with stress estimations based on simple models of topographic compensation made in the high chain of Peru (Dalmayrac & Molnar 1981) and in the Altiplano-Puna region (Froidevaux & Isacks 1984). An alternate explanation (which does not exclude the first one) for the same result is provided by mathematical estimations

of Muskhelishvili (1953), Savage, Swolfs & Powers (1985) and Savage & Swolfs (1986): the stress field expected on the near-surface of a symmetric ridge in the context of a uniform uniaxial tectonic stress acting normal to its axial plane is slightly extensional in the same direction (if the topographical gradient is enough).

In this tectonic regime, the uplift of the western Cordillera can be seen in two different ways: the compression on both sides of the belt can cause a broad, large-scale flexure of the continental crust, and consequently, the active subsidence of some areas like the Callejon de Huaylas basin: in this model, extension is mainly due to body forces produced by gravity. Another possibility may be an absolute uplift of the Cordillera Blanca batholith along a normal fault system, due to buoyancy forces originated in an isostatic adjustment of the crustal root. Soulas (1978) has already proposed a similar model to explain the very important vertical throws observed in the Cordillera Blanca. An argument for such an hypothesis is the very young age of the Cordillera Blanca batholith with respect to the other ones situated west of it (i.e. the Cordillera Negra and the Coastal batholiths). Absolute geodesic measurements are needed to have a better idea on the subject.

These two scenarios can be included in the model of Andean building proposed by Suarez *et al.* (1983). In this scenario, the authors assumed a delicate balance between the compressive forces applied to the flank of the Andes and the gravitational force applied to the elevated crust and its thickened root: thus new faults are successively created farther east when a critical height is reached, and extension occurs in these western elevated parts. We suggest that extensional effects observed at the surface in the Andean range may be greatly increased by the active ascension of young plutonic bodies intruded in the crust: this phenomenon might explain why some parts of the high Andes still should have increasing elevations.

ACKNOWLEDGMENTS

This work forms part of a Franco-Peruvian cooperation between 'Institut Français de Recherche Scientifique pour le Développement en Coopération' (ORSTOM) and 'Instituto Geofísico del Perú' (IGP). Many thanks to L. Ocola who organized the IGP assistance and to J. Tavera, A. Garro, R. Hanco, R. Lindo (IGP) and J. Berrospi (ORSTOM) for helping us during the fieldwork. L. Rivera kindly made available his programs to compute stress tensors and fault plane solutions. We are grateful to A. Cisternas for useful comments on the manuscript and to E. Jimenez (IPG Strasbourg) who made the inversion of the Ancash earthquake. Financial support for the fieldwork was provided by ORSTOM.

REFERENCES

- Aki, K., 1984. Asperities, barriers, characteristics earthquakes and strong motion prediction, *J. geophys. Res.*, **89**, 5867-5872.
- Angelier, J. & Mechler, P., 1977. Sur une méthode graphique de recherche des contraintes principales également utilisable en tectonique et en sismologie: la méthode des dièdres droits, *Bull. Soc. Geol. Fr.*, **XIX**, 1309-1218.
- Armijo, R., Carey, E. & Cisternas, A., 1982. The inverse problem

- in microtectonics and the separation of tectonic phases, *Tectonophysics*, **82**, 145–160.
- Armijo, R., Tapponnier, P., Mercier, J. L. & Tong-Lin, H., 1986. Quaternary extension in southern Tibet: field observations and tectonic implications, *J. geophys. Res.*, **91**, 13803–13872.
- Bonnot, D., 1984. Néotectonique et tectonique active de la Cordillère Blanche et du Callejon de Huaylas (Andes nord-péruviennes), *Thesis 3^e cycle*, Université Paris-Sud, 123 pp.
- Brillinger, D. R., Udias, A. & Bolt, B. A., 1980. A probability model for regional focal mechanism solutions, *Bull. seism. Soc. Am.*, **70**, 149–170.
- Carey-Gailhardis, E. & Mercier, J. L., 1987. A numerical method for determining the state of stress using focal mechanisms of earthquake populations: application to Tibetan teleseisms and microseismicity of southern Peru, *Earth planet. Sci. Lett.*, **82**, 165–179.
- Chen, W. P. & Molnar, P., 1983. Focal depths of intracontinental and intraplate earthquakes and their implications for the thermal and mechanical properties of the lithosphere, *J. geophys. Res.*, **88**, 4183–4214.
- Chinn, D. S. & Isacks, B. L., 1983. Accurate source depths and focal mechanisms of shallow earthquakes in western south America and in the New Hebrides island arc, *Tectonics*, **6**, 529–563.
- Cobbing, E. J. & Pitcher, W. S., 1972. The coastal batholith of central Peru, *J. geol. Soc. London*, **128**, 421–460.
- Couch, R., Whitsett, R. M., Huehn, B. & Briceno-Guarupe, L., 1981. Structure of the continental margin of Peru and Chile, Nazca plate, *Mem. geol. Soc. Am.*, **154**, 703–726.
- Cunningham, P. S., Roecker, S. W. & Hatzfeld, D., 1986. Three-dimensional P- and S-wave velocity structures of southern Peru and their tectonic implications, *J. geophys. Res.*, **91**, 9517–9532.
- Dalmayrac, B., 1974. Un exemple de tectonique vivante: le failles subactuelles du pied de la Cordillère Blanche (Perou), *Cah. ORSTOM, Ser. Geol.* **VI/1**, 19–27.
- Dalmayrac, B., 1978. Géologie des Andes péruviennes: Géologie de la Cordillère orientale et de la région de Huanuco: sa place dans une transversale des Andes du Pérou Central (9°S–10°30'S), *Trav. Doc. ORSTOM* **93**.
- Dalmayrac, B. & Molnar, P., 1981. Parallel thrust and normal faulting in Peru and constraints on the state of stress, *Earth planet. Sci. Lett.*, **55**, 473–481.
- Dalziel, I. W. D., 1986. Collision and Cordilleran orogenesis: an andean perspective, in *Collision Tectonics*, pp. 389–404, eds Coward, M. P. & Ries, A. C. Blackwell Scientific Publications, Oxford.
- Dorbath, C., Dorbath, L., Cisternas, A., Deverchère, J., Diamant, M., Ocola, L. & Morales, M., 1986. On crustal seismicity of the amazonian foothill of the central peruvian Andes, *Geophys. Res. Lett.*, **13**, 1023–1026.
- Doser, D. I., 1987. The Ancash, Peru, earthquake of 1946 November 10: evidence for low-angle normal faulting in the high Andes of northern Peru, *Geophys. J. R. astr. Soc.*, **91**, 57–71.
- Froidevaux, C. & Isacks, B. L., 1984. The mechanical state of the Altiplano–Puna segment of the Andes, *Earth planet. Sci. Lett.*, **71**, 305–314.
- Gephart, J. W. & Forsyth, D. W., 1984. An improved method for determining the regional stress tensor using earthquake focal mechanism data: application to the San Fernando earthquake sequence, *J. geophys. Res.*, **89**, 9305–9320.
- Giletti, B. J. & Day, H. W., 1968. Potassium–argon ages of igneous intrusive rocks in Peru, *Nature*, **220**, 570–572.
- Grange, F., Hatzfeld, D., Cunningham, P., Molnar, P., Roecker, S. W., Suarez, G., Rodrigues, A. & Ocola, L., 1984. Tectonic implications of the microearthquake seismicity and fault plane solutions in southern Peru, *J. geophys. Res.*, **89**, 6139–6152.
- James, D. E., 1971. Andean crustal and upper mantle structure, *J. geophys. Res.*, **76**, 3246–3271.
- Jimenez, E., Cara, M. & Rouland, D., 1988. Focal mechanisms of moderate-size earthquakes from the analysis of single station 3-component surface-wave records. *Bull. seism. Soc. Am.*, 1989.
- Jordan, T. E., Isacks, B. L., Allmendinger, R. W., Brewer, J. A., Ramos, V. A. & Ando, C. J., 1983. Andean tectonics related to geometry of subducted Nazca plate, *Geol. Soc. Am. Bull.*, **94**, 341–361.
- Klein, F. W., 1978. Hypocentre location program HYPOINVERSE, US Geological Survey, Open File Report 78–694.
- McKenzie, D. P., 1969. The relation between fault plane solutions for earthquakes and the directions of the principal stresses, *Bull. seism. Soc. Am.*, **59**, 591–601.
- Mégard, F., 1984. The Andean orogene period and its major structures in central and northern Peru, *J. geol. Soc. London*, **141**, 893–900.
- Mégard, F., 1987. Cordilleran Andes and marginal Andes: a review of andean geology north of the Arica elbow (18°S), in *Circum-Pacific Orogenic Belts and Evolution of the Pacific Ocean*, pp. 71–95, eds Monger, J. W. & Francheteau, J., *Geodyn. Ser.*, **18**, AGU, Washington DC.
- Mégard, F. & Philip, H., 1976. Plio–Quaternary tectono-magmatic zonation and plate tectonics in the Central Andes, *Earth planet. Sci. Lett.*, **33**, 231–238.
- Mercier, J. L., Armijo, A., Tapponnier, P., Carey-Gailhardis, E. & Tong Lin, H., 1987. Change from late tertiary compression to quaternary extension in southern Tibet during the India–Asia collision, *Tectonics*, **6**, 275–304.
- Molnar, P. & Tapponnier, P., 1978. Active tectonics of Tibet, *J. geophys. Res.*, **83**, 5361–5375.
- Muskhelishvili, N. I., 1953. *Some Basic Problems of the Mathematical Theory of Elasticity*, Noordhoff, Leiden, Netherlands.
- Rivera, L. A. & Cisternas, A., 1987. Stress tensor and fault planes solutions for a population of earthquakes, European Geophys. Soc. XII, in *Terra Cognita*, **7**, 2–3, open session (abstract), OI.2–8, 461.
- Savage, W. Z., Swolfs, H. S. & Powers, P. S., 1985. Gravitational stresses in long symmetric ridges and valleys, *Int. J. Rock Mech. Min. Sci. Geomech. Abstract*, **22**, 291–302.
- Savage, W. Z. & Swolfs, H. S., 1986. Tectonic and gravitational stress in long symmetric ridges and valleys, *J. geophys. Res.*, **91**, 3677–3685.
- Sévrier, M., Mercier, J. L., Mégard, F., Laubacher, G. & Carey-Gailhardis, E., 1985. Quaternary normal and reverse faulting and the state of stress in the central Andes of south Peru, *Tectonics*, **7**, 739–780.
- Silgado, E., 1951. The Ancash, Peru, earthquake of 1946 November 10, *Bull. seism. Soc. Am.*, **41**, 83–89.
- Soulas, J. P., 1978. Tectonique quaternaire: la côte Pacifique et la chaîne andine du Pérou central, *Rev. Géogr. Phys. Géol. Dyn.* (2), **XX**, 399–414.
- Stauder, W., 1975. Subduction of the Nazca plate under Peru as evidenced by focal mechanisms and by seismicity, *J. geophys. Res.*, **80**, 1053–1064.
- Stewart, J. W., Evernden, J. F. & Snelling, N. J., 1974. Age determinations from andean Peru: a reconnaissance survey, *Geol. Soc. Am. Bull.*, **85**, 1107–1116.
- Suarez, G., Molnar, P. & Burchfiel, B. C., 1983. Seismicity, fault plane solutions, depth of faulting and active tectonics of the Andes of Peru, Ecuador and southern Colombia, *J. geophys. Res.*, **88**, 403–423.
- Tapponnier, P., Peltzer, G. & Armijo, R., 1986. On the mechanics of collision between India and Asia, in *Collision Tectonics*, pp. 115–157, eds Coward, M. P. & Ries, A. C., Blackwell Scientific Publications, Oxford.
- Wilson, J. J., Reyes, L. & Garayar, J., 1967. Geologia de los cuadrangulos de Mollebamba, Tayabamba, Huaylas, Pomabamba, Carhuaz y Huari, *Bol. Serv. Geol. Min. Lima*, **16**, 95 pp.
- Yonekura, N., Matsuda, T., Nogami, M. & Kaizuka, S., 1979. An active fault along the western part of the Cordillera Blanca, Peru, *J. Geogr.*, **88**, 1–19.